iScience

CellPress
OPEN ACCESS

Article

Envelope virus-mimetic nanovaccines by hybridizing bioengineered cell membranes with bacterial vesicles

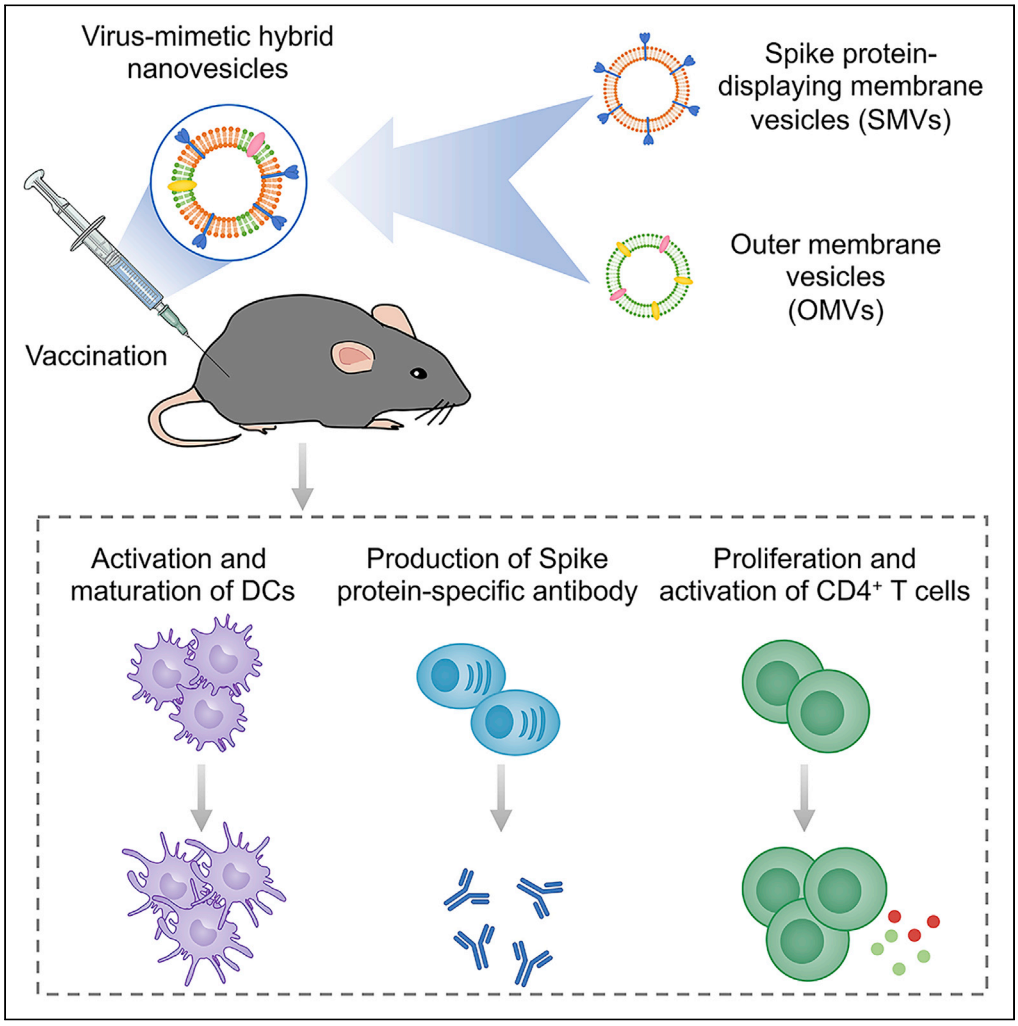

Mengmeng Zhang, Lu Wang, Jinyao Liu, Yan Pang

jyliu@sjtu.edu.cn (J.L.)
yanpang@shsmu.edu.cn (Y.P.)

Highlights

Nanovaccines were hybridized by bioengineered cell membranes and bacterial vesicles

Nanovaccines possessed intact viral antigens with natural conformation

Nanovaccines promoted antigen uptake, processing, and presentation by dendritic cells

Nanovaccines elicited robust humoral and cellular immune responses in mice

Zhang et al., iScience 25, 104490
June 17, 2022
https://doi.org/10.1016/j.isci.2022.104490

iScience

CellPress
OPEN ACCESS

Article

Envelope virus-mimetic nanovaccines by hybridizing bioengineered cell membranes with bacterial vesicles

Mengmeng Zhang,[1,3] Lu Wang,[1,3] Jinyao Liu,[1,4,*] and Yan Pang[2,*]

SUMMARY

Emerging threats of rapid spread highly lethal infectious diseases highlight the urgent need of vaccine development. Here, we describe the preparation of envelope virus-mimetic nanovaccines by hybridizing bioengineered cell membranes with bacterial vesicles. Membranes acquired from bioengineered cells overexpressing viral antigens are fused with bacterial outer membrane vesicles to develop hybrid nanovesicles. Because of the presence of intact viral antigenic proteins with natural conformation bound to lipid bilayer and pathogen-associated molecular patterns, hybrid nanovesicles can strikingly promote antigen uptake, processing and presentation by dendritic cells. Immunization with envelope virus-mimetic nanovaccines shows significantly enhanced maturation and activation of dendritic cells, which elicit robust humoral and cellular immune responses in mice. By virtue of their artificial characteristic and absence of loaded adjuvants, these biomimetic nanovaccines exhibit favorable biosafety. Our work demonstrates the effectiveness of envelope virus-mimetic nanovaccines to boost antigen-specific immunity and proposes a simple yet versatile platform to prepare antiviral vaccines.

INTRODUCTION

Beginning from the end of 2019, the coronavirus disease 2019 (COVID-19) pandemic has rapidly spread worldwide (Wu et al., 2020; Zhu et al., 2020). This global pandemic has challenged the public health system and has significantly impeded the global economy (Chakraborty and Maity, 2020; Walker et al., 2020). The extremely high infection rate and majority of severe asymptomatic infections of COVID-19 spotlight the urgent need of vaccine development (Gao et al., 2020; Jeyanathan et al., 2020; Liu et al., 2020). Vaccines are an intelligent design for mobilizing the body's own immune system to fight against foreign invaders or mutation-derived neoantigens (Aurisicchio et al., 2018; Shin et al., 2020). Traditional vaccines mainly include entire attenuated living or inactivated pathogens, subunit vaccines, and nucleic acid vaccines (Zhou et al., 2020b). As is well known, the development of an effective vaccine is a long, high-cost, and complex process, which suffers from a number of limitations (Jiang et al., 2012). For example, extensive tests and evaluations are needed to ensure high immunogenicity of inactivated viruses or to avoid safety issues of live-attenuated viruses (Lycke, 2012). In addition, recombinant antigens including proteins/peptides or glycoproteins used for subunit vaccine development need complicated design and isolation processes to maintain native three-dimensional structure (Rothe et al., 2020; Wang et al., 2020). As for DNA vaccines, low immunogenicity profiles, risk of random integration into the host genome, and challenge of ensuring delivery into cell nucleus remain difficult to overcome (McKenzie et al., 2001; Pushparajah et al., 2021). Although RNA vaccines have promoted the development of nucleic acid vaccines, physiological obstacles and instability hinder their transmission and transfection efficiency (Qin et al., 2021). Therefore, alternative approaches for vaccine development are highly desirable to meet the urgency of vaccine needs (Krammer, 2020).

Incorporation with lipid membranes is an effective method to maintain the native conformation of a multimer (Ren et al., 2021). However, protein antigens have an inherent lack of efficient immunostimulation, leading to a limited antibody production (Zhou et al., 2020b). Although various adjuvants are available, formulation with protein antigens to boost immune responses often has problems with leakages, which cause potential side effects (Batista-Duharte et al., 2018; Coffman et al., 2010). Given that native

[1]Shanghai Key Laboratory for Nucleic Acid Chemistry and Nanomedicine, Institute of Molecular Medicine, State Key Laboratory of Oncogenes and Related Genes, Shanghai Cancer Institute, Renji Hospital, School of Medicine, Shanghai Jiao Tong University, Shanghai 200127, China

[2]Shanghai Key Laboratory of Orbital Diseases and Ocular Oncology, Department of Ophthalmology, Shanghai Ninth People's Hospital, School of Medicine, Shanghai Jiao Tong University, Shanghai 200011, China

[3]These authors contributed equally

[4]Lead contact

*Correspondence: jyliu@sjtu.edu.cn (J.L.), yanpang@shsmu.edu.cn (Y.P.)

https://doi.org/10.1016/j.isci.2022.104490

conformation of antigens is pivotal for priming B cells to produce highly effective neutralizing antibodies (Mond and Brunswick, 2003), cell membrane-mediated top-down approach has been reported as a facile and effective approach to retain intact antigenic information (Hu et al., 2015). Inspired by this biomimetic nanotechnology, cell membrane-derived vesicles (CMVs) have been widely employed to deliver a variety of functional proteins (Chen et al., 2019). For instance, vaccinated with cancer-derived cell membranes can inhibit tumor cells in a prophylactic study (Kroll et al., 2017). Moreover, it has been demonstrated that CMVs can display viral envelope glycoproteins by genetic engineering and mimic the properties of natural viruses (Zhang et al., 2015). Despite these elegant achievements, previous vaccines based on CMVs also require adjuvant loading, as antigen-embedded cell membranes alone are incapable of eliciting adequate immune responses. Because of the incorporation of two or more original cell membranes, fused cell membrane-derived vesicles can synergistically execute more complex activities (Chen et al., 2020c; Le et al., 2021). Bacterial outer membrane vesicles (OMVs) contain a large number of bioactive components (Jan, 2017; Lee et al., 2008; Schwechheimer and Kuehn, 2015), which can directly interact with various immune cells to comprehensively regulate immune responses (Kaparakis-Liaskos and Ferrero, 2015). OMVs released from *Salmonella* induce upregulated expressions of CD86 and major histocompatibility complex (MHC) class II molecules on dendritic cells (DCs), increased productions of tumor necrosis factor alpha (TNF-α) and interleukin-12 (IL-12), and elevated protective B cell and T cell responses (Alaniz et al., 2007; Chen et al., 2020b; Laughlin et al., 2015; Schetters et al., 2019). Incorporation with OMVs derived from *Salmonella* can facilitate melanoma CMVs to trigger an antitumor immune response (Zou et al., 2021). Thus, instead of carrying adjuvants, hybridizing with OMVs proposes an alternative to enhance the immunogenicity of CMV-based vaccines.

Here, we report envelop virus-mimetic hybrid membrane-derived vesicles (HMVs), which are prepared by fusing viral antigenic protein-displayed CMVs with OMVs released from bacteria, to induce antiviral immune responses. As a proof-of-concept study, Spike glycoprotein, a large type I transmembrane protein that can bind to angiotensin-converting enzyme 2 (ACE2) and mediate cell entry of severe acute respiratory syndrome-coronavirus 2 (SARS-CoV-2), is selected as a model viral antigen to bioengineer Spike protein-displayed CMVs (SMVs). On the other hand, OMVs secreted by attenuated *Salmonella* are chosen because of their strong immunogenicity. By virtue of the presence of intact Spike protein with native structure bound to lipid bilayer and pathogen-associated molecular patterns (PAMPs), HMVs can greatly upgrade Spike protein uptake, processing and presentation by DCs. Vaccination with HMVs can boost both humoral and cellular immune responses in mice. Specifically, compared to corresponding individual components, HMVs significantly promote the activation of B cells, proliferation of T cells, maturation of DCs, and production of antigen-specific antibodies. Benefiting from the artificial feature and absence of adjuvant loading, envelope virus-mimetic nanovaccines show favorable biosafety and tolerance, as implied by negligible fluctuation in mouse body weight following immunization. In light of the maturity of genetic engineering to express diverse antigenic proteins, we anticipate the use of hybridizing bioengineered cell membranes with bacterial vesicles as a facile yet universal platform to prepare effective subunit vaccines for preventing infectious diseases.

RESULTS

Preparation and characterization of HMVs

Human embryonic kidney (HEK) 293T cell line has been extensively used to express high amounts of recombinant proteins with proper protein folding and post-translational modifications (Thomas and Smart, 2005). Here, we chose Spike protein overexpressed HEK 293T cells as the source of SARS-CoV-2 antigen through genetic engineering (Table S1). Western blot analysis indicated a successful transfection and expression of Spike protein in HEK 293T cells (Figure S1). By staining with fluorescent antibodies, flow cytometric (FCM) analysis proved that Spike protein was successfully displayed on the surface of HEK 293T cells (Figure S2). SMVs were then obtained from engineered HEK 293T cells via hypotonic lysis and differential centrifugation. OMVs were isolated and purified from the culture medium of attenuated *Salmonella* by ultracentrifugation. HMVs were fabricated by fusing SMVs with OMVs at a ratio of 10:1 in phosphate buffer solution (PBS) via ultrasonic fusion and membrane extrusion (Figure 1A). Transmission electron microscopy (TEM) images revealed the spherical structures of HMVs after negatively staining with phosphotungstic acid hydrate (Figure 1B). The average diameter of HMVs was approximately 167.5 $\pm$ 2.3 nm as demonstrated by dynamic light scattering (DLS) analysis, which also showed a zeta potential around −11 mV (Figures 1C, 1D, and S3). DiO-labeled SMVs and Cy5.5-marked OMVs were used to further verify the successful fusion of vesicles. The effective fusion was confirmed by confocal laser scanning microscopy (CLSM), showing

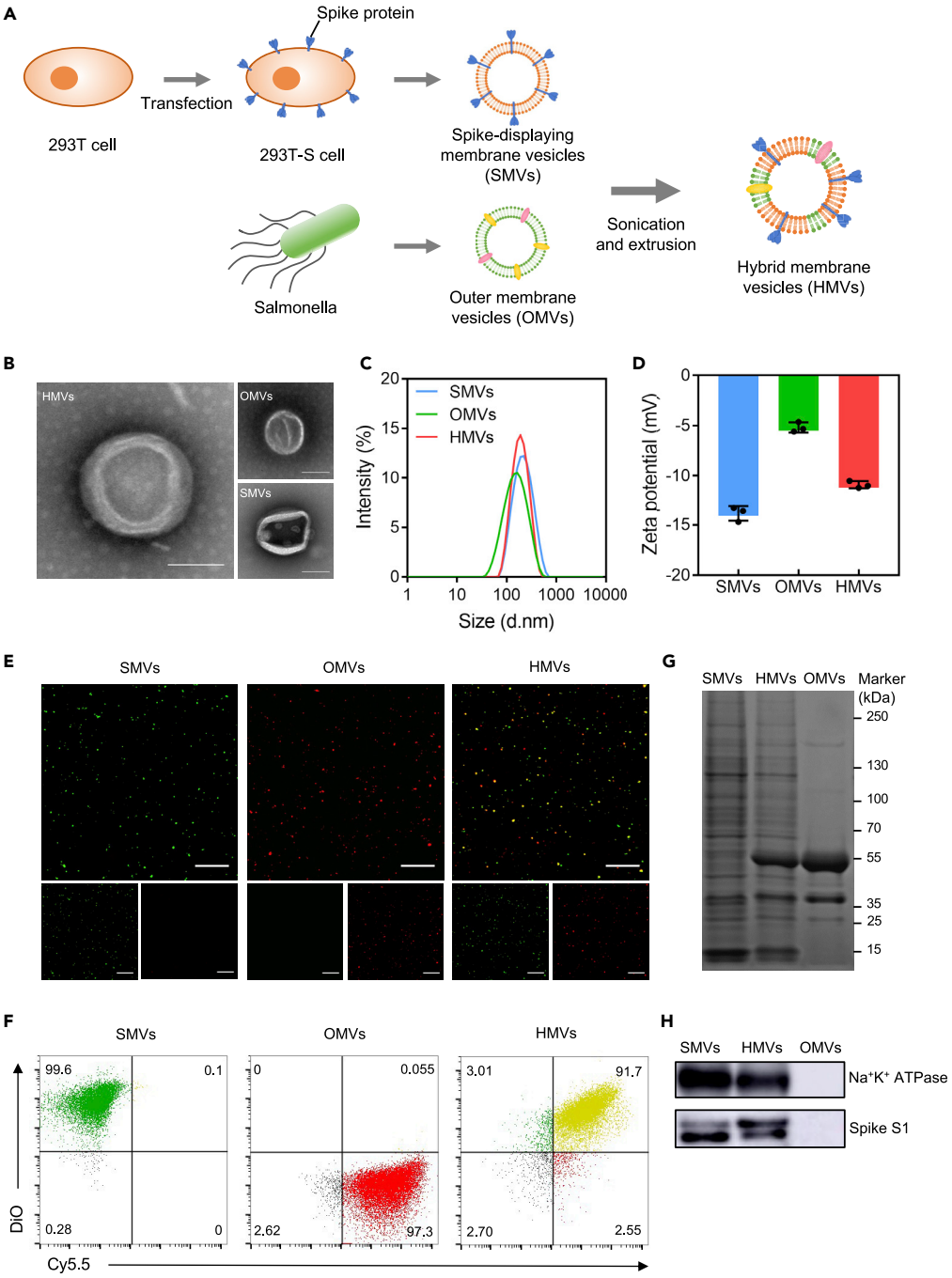

Figure 1. Characterization of HMVs

(A) Schematic illustration of preparation of HMVs. See also Figures S1 and S2 and Table S1.

(B) TEM images of SMVs, OMVs, and HMVs negatively stained with phosphotungstic acid hydrate. Scale bar: 100 nm. See also Figure S3.

(C and D) Hydrodynamic size and (D) surface zeta potential of SMVs, OMVs, and HMVs measured by DLS. Data are shown as means ± SD (n = 3). See also Figure S4.

(E) CLSM images of SMVs labeled with DiO (green), OMVs stained with Cy5.5 (red), and HMVs. Scale bar: 10 μm.

(F) FCM analysis of SMVs marked with DiO, OMVs labeled with Cy5.5, and HMVs.

(G) SDS-PAGE protein analysis of SMVs, OMVs, and HMVs. Numbers indicate estimated molecular weight in kilodaltons (kDa).

(H) Detection of S1 protein from SMVs, OMVs, and HMVs by western blots. Na^+K^+ ATPase was selected as a plasma membrane loading control. See also Figure S5.

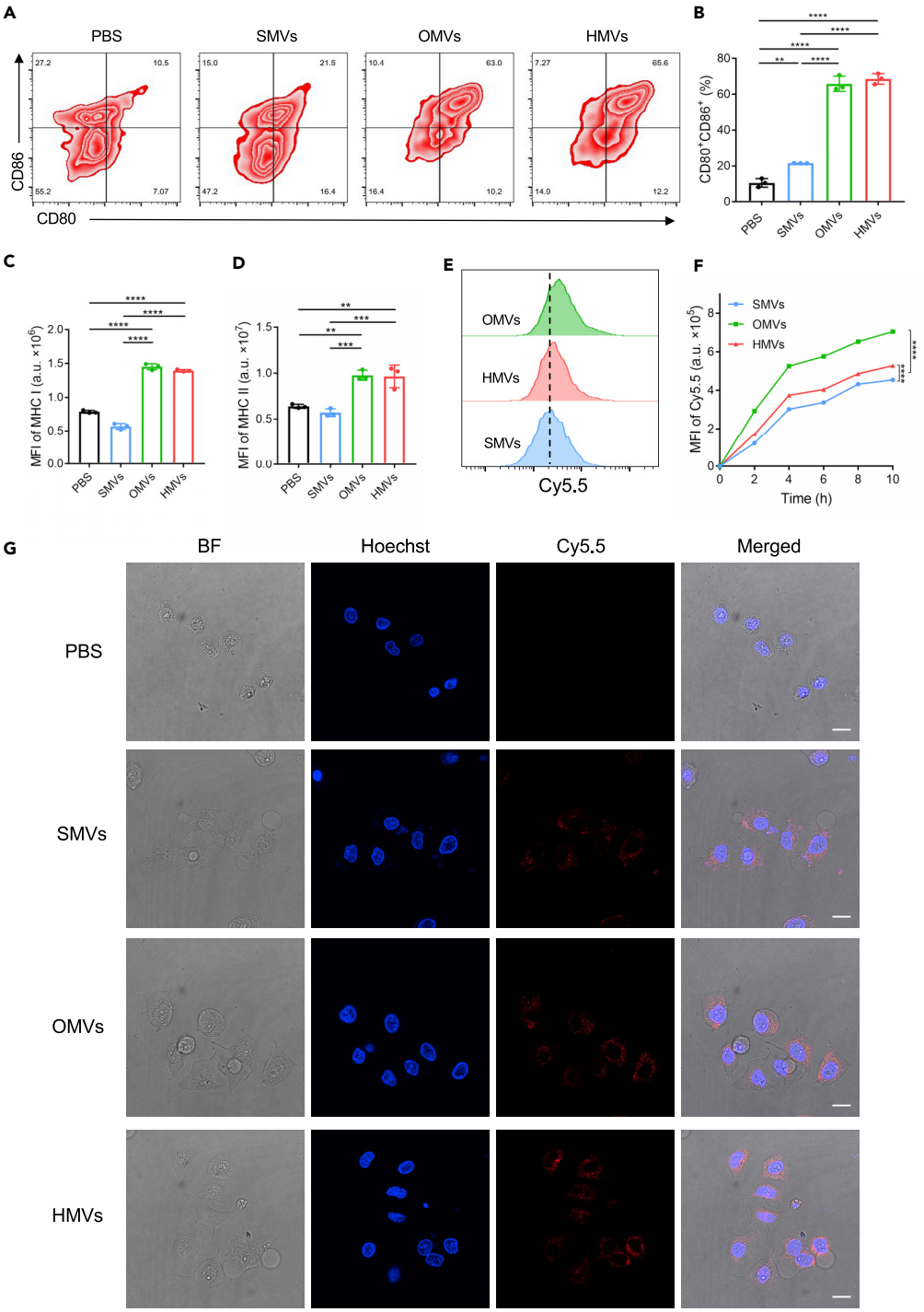

Figure 2. DCs activation and uptake *in vitro*

BMDCs were separately incubated with SMVs, OMVs, and HMVs for 24 h and analyzed by FCM.

(A–D) Scatterplots and (B) quantified percentages of $CD80^{+}CD86^{+}$ BMDCs. Mean fluorescence intensity (MFI) quantification of (C) MHC I and (D) MHC II on the surface of BMDCs. DC2.4 cells were incubated with Cy5.5-labeled SMVs, OMVs, and HMVs, respectively.

(E) FCM histograms of DC2.4 cells after incubation for 4 h.

Figure 2. *Continued*
(F) Kinetics of MFI of DC2.4 cells over 10 h after incubation.
(G) CLSM images of DC2.4 cells after incubation for 10 h. BF represents a bright field. Scale bars: 20 μm. Data are shown as means ± SD (n = 3). Statistical analysis was performed using one-way ANOVA with the Tukey's post-test and two-way ANOVA with the Bonferroni correction post-test; **p < 0.01, ***p < 0.001, ****p < 0.0001.

colocalized fluorescence signals in HMVs (Figure 1E). FCM quantification implied an adequate fusion rate of these vesicles as the degree of double-positive events was as high as 91% (Figure 1F). Sodium dodecyl sulfate-polyacrylamide gel electrophoresis (SDS-PAGE) was conducted to confirm the presence of proteins from both types of vesicles. It was noted that HMVs reserved most of the proteins existing in SMVs and OMVs. Western blot analysis revealed that Spike protein was expressed on SMVs and HMVs, whereas no signal was detected from OMVs (Figures 1H and S4). These results expounded the successful fusion of SMVs and OMVs.

Enhanced maturation and activation of APCs by HMVs

DCs play a critical role in initiating T cell-mediated cellular immunity and T cell-dependent antibody production (MacLennan and Vinuesa, 2002). Upon antigen uptake, immature DCs upregulate expressions of MHC and co-stimulatory molecules on their surface (Palucka and Banchereau, 2012). To assess their immunostimulatory ability, bone marrow-derived dendritic cells (BMDCs) were incubated with SMVs, OMVs, and HMVs, respectively. After an overnight cocultivation, the cells were collected and analyzed by FCM. Compared with the PBS group, treatment with SMVs indicated a mild increase in percentage of mature BMDCs ($CD80^+CD86^+$) (Figures 2A and 2B). Notably, the percentage of mature BMDCs for HMVs was 65.6%, which was obviously higher than that of SMVs (21.5%), but comparable to OMVs (63.0%) (Figures 2A and 2B), implying the role of OMVs as a potent adjuvant. Furthermore, MHC I and MHC II molecules on DCs are essential for the adaptive immune system, which presents foreign peptides to cytotoxic T cells and helper T cells, respectively (Villadangos and Schnorrer, 2007). Expression levels of MHC I and MHC II molecules on BMDCs incubated with SMVs changed insignificantly compared to the PBS group (Figures 2C and 2D). Fusion with OMVs contributed to a greater increase in MHC expression than treatment with SMVs alone (Figures 2C and 2D), which demonstrated that OMVs could significantly promote antigen presentation.

To elucidate the possible mechanisms that HMVs promoted DCs maturation and antigen presentation, cells were incubated with Cy5.5-labeled SMVs, OMVs, and HMVs. The uptake by DCs was evaluated by FCM. As expected, DCs treated with OMVs and HMVs exhibited a dramatic shift to the right of histogram in comparison to SMVs (Figure 2E), illustrated more OMVs and HMVs were internalized by DCs. In addition, quantitative analysis showed fluorescence intensity increased with incubation time (Figure 2F). Typical CLSM images showed that Cy5.5-labeled OMVs and HMVs were rapidly endocytosed into the cytoplasm of DCs after 10 h of coincubation, further supporting the results of FCM (Figure 2G). Thus, the incorporation of OMVs with SMVs could significantly increase the uptake of antigen by DCs and benefit further maturation and antigen presentation.

Improved humoral and cellular immune responses

To further validate the potential of HMVs in promoting immunogenicity, we performed *in vivo* experiments in mice. As illustrated in Figure 3A, mice were injected intramuscularly with PBS, OMVs, SMVs, and HMVs, respectively. Given that antibodies are crucial to eliminate invading pathogens by direct neutralization, serum was collected on day 14, 21, and 28 for immunoglobulin G (IgG) antibodies assessment. Mice administered with HMVs evoked significantly higher levels of Spike-specific IgG than those of other groups (Figure 3B). The ratio of IgG1 to IgG2a was calculated as it could reflect the bias in T helper type-2 (Th2) and T helper type-1 (Th1) immune responses (Chung et al., 2021). Among all these groups, an increase of IgG1/IgG2a ratio was observed in HMVs-treated mice, indicating the dominantly Th2-mediated humoral response (Figure 3C). Clonal expansion and activation of antigen-specific B cells is prominent for antibodies production and protective immunity induction (Nothelfer et al., 2015). As shown in Figure 3D, only HMVs treatment increased the percentage of Spike-specific B cells by analyzing splenocytes at day 30. In addition, HMVs group generated a more significantly promoted activation of B cells than other controls (Figure 3E). These results suggested that HMVs could induce effective humoral immune responses.

Considering that cellular immunity also acts as a powerful weapon against pathogens, we assessed whether HMVs could elicit T cell responses. Ki67 is a reliable marker of cellular turnover, thereby

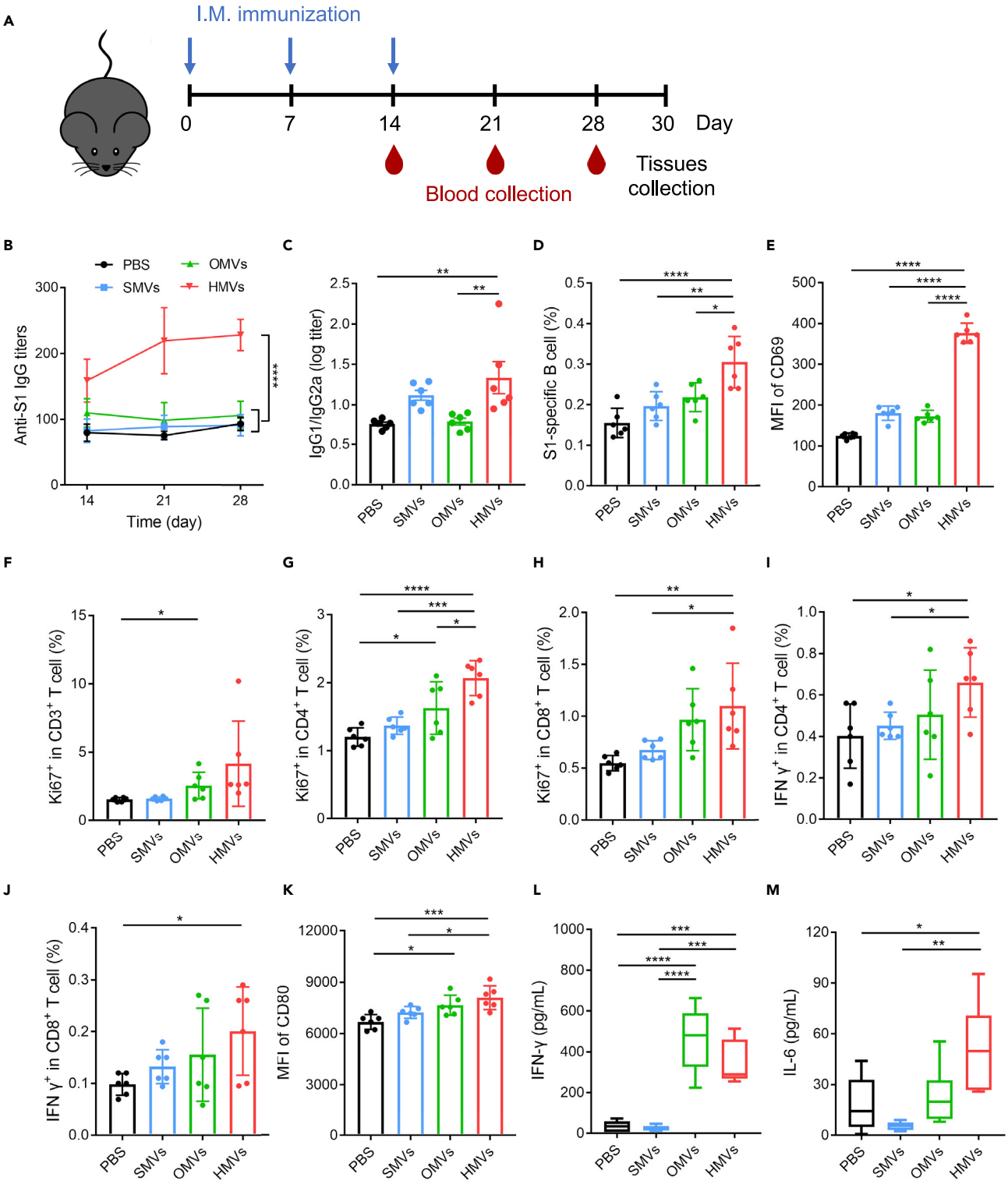

Figure 3. Immune responses in HMVs-vaccinated mice

(A) Schematic diagram of experimental designs for immunization and sample collection.

(B and C) Kinetics of IgG antibody titers to SARS-CoV-2 S1 and (C) ratio of IgG1/IgG2a at day 28 in serum assessed by enzyme-linked immunosorbent assay (ELISA).

(D and E) Percentage of SARS-CoV-2 S1-specific B cells and (E) MFI quantification of CD69 on B cells in splenocytes analyzed by FCM.

Figure 3. *Continued*

(F–J) Total T cells, (G, I) $CD4^+$ T cells, and (H, J) $CD8^+$ T cells responses in the spleen evaluated by intracellular IFN-γ and Ki67 staining. (K) MFI quantification of CD80 on DCs in splenocytes analyzed by FCM.

(L and M) IFN-γ and (M) IL-6 levels in serum measured by ELISA. Data are shown as means ± SD (n = 6). Statistical analysis was performed using one-way ANOVA with the Tukey's post-test and two-way ANOVA with the Bonferroni correction post-test; *p < 0.05, **p < 0.01, ***p < 0.001, ****p < 0.0001. See also Figure S6.

reflecting the level of T cell activation during infection (Sachsenberg et al., 1998). Increased percentage of $Ki67^+$ cells in total T cells from the spleen expounded that treatment with HMVs substantially promoted the proliferation of T cells (Figure 3F). $CD4^+$ T cells subsets, which orchestrate the immune response and help prime B cells during infection (Chen et al., 2020a), performed a more significant proliferation (Figures 3G and 3H). It was worth mentioning that interferon-gamma (IFN-γ), produced primarily by activated natural killer cells, Th1 cells, and $CD8^+$ cytotoxic cells, is a pivotal moderator of cellular immunity to fight multiple pathogens (Shibuya et al., 2021). The percentages of IFN-γ-secreting cells in both $CD4^+$ and $CD8^+$ T cells subsets in mice primed with HMVs were notably higher than that in mice treated with PBS (Figures 3I and 3J), suggesting that HMVs could modulate IFN-γ-mediated immune responses. These results illustrated that HMVs could induce effective T cell-mediated immune responses. Similar to *in vitro* results, DCs from HMVs-administered mice exhibited an upgraded expression of CD80 (Figure 3K), which clarified the improved DCs maturation. Elevated secretions of IFN-γ and IL-6 in serum samples further supported that HMVs were potent to elicit a strong systemic antiviral immune response (Figures 3L and 3M).

Safety assessment

Although OMVs were derived from *Salmonella* genetically attenuated by deleting purI and msbB (Mi et al., 2019), several concerns remain regarding the safety for *in vivo* studies. Thus, we evaluated the safety of HMVs both *in vitro* and *in vivo*. To detect their cytotoxicity, DC2.4 cells were incubated with various concentrations of HMVs for 24 h and cell counting kit-8 (CCK-8) was subsequently used to assess the viability of cells. As shown in Figure 4A, the viability of cells displayed negligible influence even with concentration increasing up to 200 μg/mL. Moreover, the body weight of immunized mice was monitored every 3 days, which displayed an insignificant decrease in HMVs' group compared to other groups (Figure 4B). In addition, histological examinations by hematoxylin and eosin (H&E) staining of major organs from immunized mice were performed and the results showed no pathological abnormality or inflamed cells after HMVs treatment (Figure 4C). These results indicated favorable biosafety and tolerance of HMVs in mice.

DISCUSSION

The coronavirus, SARS-CoV-2, has caused unprecedented health and socio-economic consequences in recent years because of their high morbidity and mortality. Currently, the global spread of SARS-CoV-2 seems to continue before a high level of herd immunity appears within the human population (Coyle et al., 2021). Although vast vaccines have been developed, some of which have been approved for use, it is still hard to obtain available vaccines in middle-income and low-income countries, which severely hinder the progress achieved by currently global vaccination (Asundi et al., 2021). Thus, an effective and affordable vaccine for mass immunization of people is pivotal to fight against the COVID-19 pandemic. Subunit vaccines are noted for their safety, facile production, and high efficacy rate, because only fragments of protein from a pathogen that can be recognized by the immune system are applied (Zhou et al., 2020b). Compared with nucleic acid-based vaccines, which produce pathogenic proteins after vaccination, administration of pathogenic protein antigens seems to be more efficient and more straightforward to trigger immunity (Wang et al., 2020). With the advance of genome sequence and recombinant protein technology, the process of subunit vaccine research and development has been largely shortened. Despite the advantages of subunit vaccines, recombinant antigens are confronted with complicated time-consuming purification, difficulties of maintaining native conformational epitope structures, and requirement for adjuvants.

In this work, we developed a subunit vaccine strategy based on virus-mimetic HMVs, displaying Spike protein on the membrane surface and also containing PAMPs. Different from conventional subunit vaccines, HMVs carried natural conformation of antigens bound to lipid bilayer and could be obtained without requirement for antigen isolation and purification. Western blot and immunofluorescence

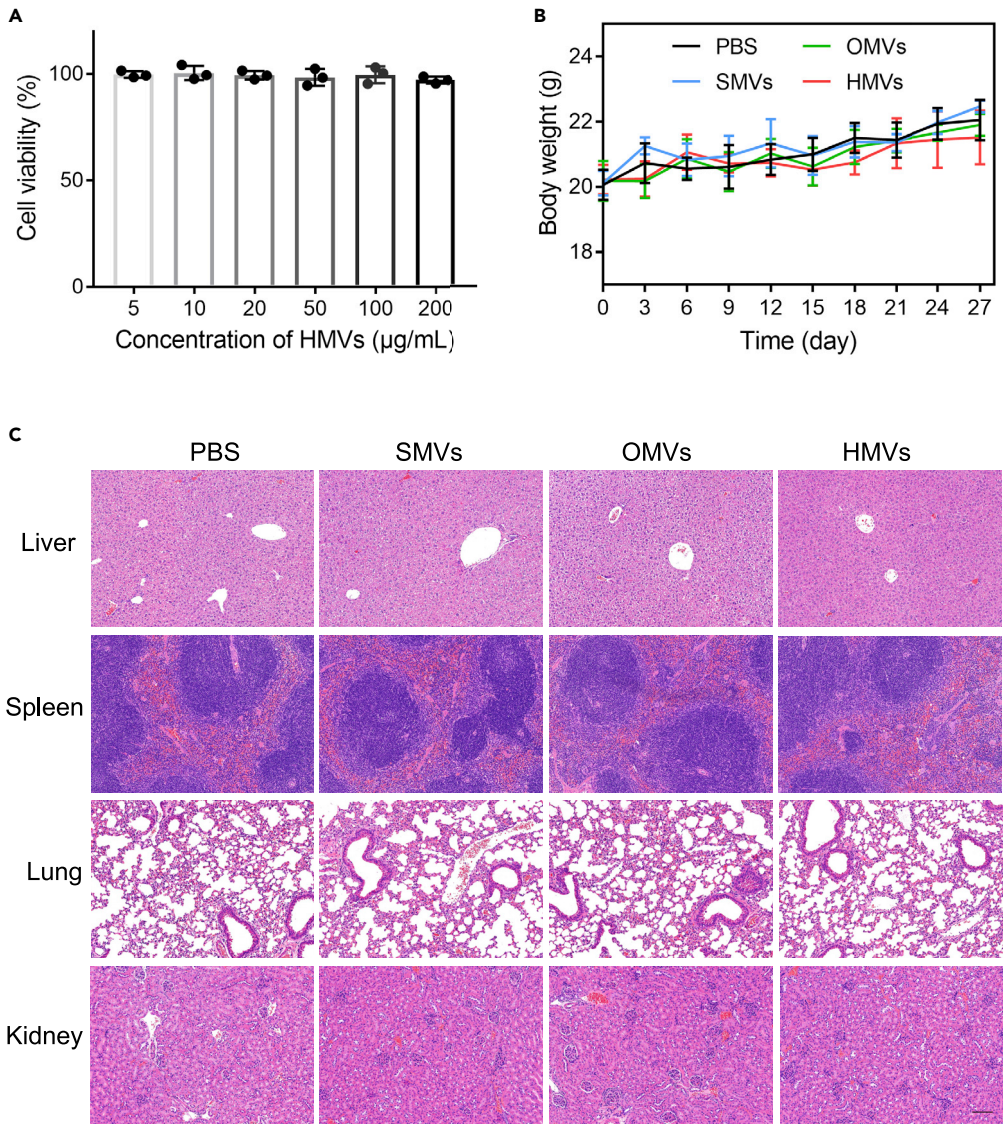

Figure 4. Biosafety evaluation

(A) Cell viability of DC2.4 cells after incubation with different concentrations of HMVs for 24 h by a CCK-8 assay. Data are shown as means ± SD (n = 3).

(B) Body weight of mice after vaccination. Data are shown as means ± SD (n = 6).

(C) H&E staining of the liver, spleen, lung, and kidney at the end of the experiment. Scale bar: 100 μm. See also Figure S7.

analysis suggested that Spike protein was successfully transfected into HEK 293T cells and maintained a correct orientation on the surface (Figures S1 and S2). Particularly, leveraging post-translational modifications of proteins, such as palmitoylation, may largely enhance cell membrane localization of Spike protein (Xie et al., 2021), which is beneficial to further elevate antibody levels. Furthermore, instead of loading with adjuvants, inherent immunogenicity of pathogenic components associated with fused OMVs was able to provoke strong immune responses. In addition, HMVs possessed a size similar to SARS-CoV-2, approximately ranging from 50 to 150 nm in diameter (Ehtezazi et al., 2021). Upon vaccination with HMVs, strong humoral and cellular responses were activated in mice. Given the presence of Spike protein on the surface, SMVs theoretically exhibited a similar pathway to enter host cells by binding to ACE2 receptors (Zhou et al., 2020a). However, human monocyte-derived DCs that rarely express ACE2 have not been infected after exposure to SARS-CoV-2 isolate (van der Donk et al., 2021). Neither SARS-CoV-2 isolate nor S protein alone could induce DC maturation, which was consistent with our

observations (Figures 2A–2D). Therefore, we hypothesized that SMVs entered DCs as extracellular vesicles through endocytic pathways (Mulcahy et al., 2014). Notably, fusion with OMVs remarkably elevated the uptake of HMVs by DCs (Figures 2E–2G), which may be caused by lipopolysaccharide (LPS) and O antigen associated with OMVs (Gu et al., 2019; O'Donoghue et al., 2017). Indeed, PAMPs, such as LPS, lipoprotein, peptidoglycan or nucleic acids from OMVs, contributed to the induction of DC maturation (Figures 2A–2D). Although vaccines could disseminate from the injection site to blood vessels in muscle and further into the spleen to induce systemic immune responses, studies have shown that intramuscular injection of vaccines could lead to a rapid accumulation from the injection site to the draining lymph nodes (dLNs), where local immune responses were induced (Ols and Loré, 2019). Thus, we detected the activation of T cells in dLNs, which displayed a primary proliferation of $CD4^+$ T cells subset in HMVs-treated mice (Figure S5). Furthermore, PAMPs from OMVs may be a double-edged sword for vaccination, suggesting that immunization benefits and tissue damages should be balanced. To this end, we attempted to fuse SMVs with OMVs at a ratio of 10:1 or 100:1 for *in vivo* experiments. After treatment with HMVs containing 10% OMVs, mice lost approximately 10% of body weight, accompanied by inappetence, withered hair, and slow in action (Figure S6). Most importantly, antibodies in serum were undetectable. With the proportion of OMVs in HMVs reducing to 1%, we found that vaccination had limited influence on mouse body weight and induced more effective immune responses (Figures 3 and 4B). Moreover, HMVs with 1% loading of OMVs verified negligible cytotoxicity and tissue damages (Figures 4A and 4C). Currently, detergent extraction is usually conducted in licensed OMV-based vaccines to reduce LPS-mediated toxicity (Balhuizen et al., 2021), which may be used to regulate appropriate immunogenicity of HMVs for future translation.

In summary, we have constructed a biomimetic platform capable of preparing virus-mimicking nanovaccines for preventing viral infection. By simply hybridizing CMVs that are bioengineered to overexpress virus-specific antigens with bacterial OMVs, hybrid nanovesicles that present intact antigen structure with inherent conformation bound to lipid bilayer and PAMPs can be obtained successfully. For proof-of-principle, CMVs displaying Spike protein are fused with OMVs derived from *Salmonella* to generate virus-mimicking nanovaccines. In addition to their favorable biosafety and tolerance, hybrid nanovesicles can potently stimulate antigen processing and presentation by DCs, T cell activation, and antibody production, along with inflammatory cytokine release. More significantly, this flexible platform can be potentially extended to develop diverse nanovaccines for preventing other infectious diseases by altering antigen expression, even to fabricate polyvalent vaccines for more effective protection.

Limitations of the study

Although we demonstrate that vaccination with HMVs can produce protective immune responses in mice, the dose and frequency of administration needs to be optimized. The activation of antigen-specific T cells has not been assessed because of technical issues. These limitations will be explored deeply in future studies before further translation.

STAR★METHODS

Detailed methods are provided in the online version of this paper and include the following:

- KEY RESOURCES TABLE
- RESOURCE AVAILABILITY
  - Lead contact
  - Materials availability
  - Data and code availability
- EXPERIMENTAL MODEL AND SUBJECT DETAILS
  - Cell culture and transfection with spike protein
  - Bacterial culture and OMVs collection
  - Cell viability assay
  - Cell uptake *in vitro*
  - Maturation and activation of BMDCs *in vitro*
  - Mice vaccination
- METHOD DETAILS
  - Flow cytometric analysis of spike protein expression
  - Preparation of SMVs and HMVs

- Characterization of SMVs, OMVs, and HMVs
- ELISA for serum antibody titer evaluation
- Immune responses and flow cytometric analysis *in vivo*
- ELISA for detection of cytokines in serum
- Histopathology assay

- QUANTIFICATION AND STATISTICAL ANALYSIS

SUPPLEMENTAL INFORMATION

Supplemental information can be found online at https://doi.org/10.1016/j.isci.2022.104490.

ACKNOWLEDGMENTS

This work was financially supported by the National Key Basic Research Program (SQ2021YFA090162), the National Natural Science Foundation of China (21875135), the Innovative Research Team of High-Level Local Universities in Shanghai (SHSMU-ZDCX20210900, SHSMU-ZDCX20210700), the Science and Technology Commission of Shanghai (20DZ2270800), and the Two-hundred Talent (20191820).

AUTHOR CONTRIBUTIONS

M.M.Z. and L.W. contributed equally to this work; Y.J.L. and Y.P. supervised the project; M.M.Z. and L.W. performed experiments and data analysis; All authors wrote and approved the manuscript.

DECLARATION OF INTERESTS

The authors declare no competing interests.

Received: February 15, 2022
Revised: April 18, 2022
Accepted: May 20, 2022
Published: June 17, 2022

REFERENCES

Alaniz, R.C., Deatherage, B.L., Lara, J.C., and Cookson, B.T. (2007). Membrane vesicles are immunogenic facsimiles of Salmonella typhimurium that potently activate dendritic cells, prime B and T cell responses, and stimulate protective immunity in vivo. J. Immunol. *179*, 7692–7701. https://doi.org/10.4049/jimmunol.179.11.7692.

Asundi, A., O'Leary, C., and Bhadelia, N. (2021). Global COVID-19 vaccine inequity: the scope, the impact, and the challenges. Cell Host Microbe *29*, 1036–1039. https://doi.org/10.1016/j.chom.2021.06.007.

Aurisicchio, L., Pallocca, M., Ciliberto, G., and Palombo, F. (2018). The perfect personalized cancer therapy: cancer vaccines against neoantigens. J. Exp. Clin. Cancer Res. *37*, 86. https://doi.org/10.1186/s13046-018-0751-1.

Balhuizen, M.D., Veldhuizen, E.J.A., and Haagsman, H.P. (2021). Outer membrane vesicle induction and isolation for vaccine development. Front. Microbiol. *12*, 629090. https://doi.org/10.3389/fmicb.2021.629090.

Batista-Duharte, A., Martínez, D.T., and Carlos, I.Z. (2018). Efficacy and safety of immunological adjuvants. where is the cut-off? Biomed. Pharmacother. *105*, 616–624. https://doi.org/10.1016/j.biopha.2018.06.026.

Chakraborty, I., and Maity, P. (2020). COVID-19 outbreak: migration, effects on society, global environment and prevention. Sci. Total Environ. *728*, 138882. https://doi.org/10.1016/j.scitotenv.2020.138882.

Chen, Z.W., Wang, Z.J., and Gu, Z. (2019). Bioinspired and biomimetic nanomedicines. Acc. Chem. Res. *52*, 1255–1264. https://doi.org/10.1021/acs.accounts.9b00079.

Chen, D.Y., Wolski, D., Aneja, J., Matsubara, L., Robilotti, B., Hauck, G., de Sousa, P.S.F., Subudhi, S., Fernandes, C.A., Hoogeveen, R.C., et al. (2020a). Hepatitis C virus-specific CD4+ T cell phenotype and function in different infection outcomes. J. Clin. Invest. *130*, 768–773. https://doi.org/10.1172/jci126277.

Chen, Q., Bai, H.Z., Wu, W.T., Huang, G.J., Li, Y., Wu, M., Tang, G.P., and Ping, Y. (2020b). Bioengineering bacterial vesicle-coated polymeric nanomedicine for enhanced cancer immunotherapy and metastasis prevention. Nano Lett. *20*, 11–21. https://doi.org/10.1021/acs.nanolett.9b02182.

Chen, Q., Huang, G.J., Wu, W.T., Wang, J.W., Hu, J.W., Mao, J.M., Chu, P.K., Bai, H.Z., and Tang, G.P. (2020c). A hybrid eukaryotic-prokaryotic nanoplatform with photothermal modality for enhanced antitumor vaccination. Adv. Mater. *32*, e1908185. https://doi.org/10.1002/adma.201908185.

Chung, N.-H., Chen, Y.-C., Yang, S.-J., Lin, Y.-C., Dou, H.-Y., Hui-Ching Wang, L., Liao, C.-L., and Chow, Y.-H. (2021). Induction of Th1 and Th2 in the protection against SARS-CoV-2 through mucosal delivery of an adenovirus vaccine expressing an engineered spike protein. Vaccine *40*, 574–586. https://doi.org/10.1016/j.vaccine.2021.12.024.

Coffman, R.L., Sher, A., and Seder, R.A. (2010). Vaccine adjuvants: putting innate immunity to work. Immunity *33*, 492–503. https://doi.org/10.1016/j.immuni.2010.10.002.

Coyle, P.V., Chemaitelly, H., Ben Hadj Kacem, M.A., Abdulla Al Molawi, N.H., El Kahlout, R.A., Gilliani, I., Younes, N., Al Anssari, G.A.A.A., Al Kanaani, Z., Al Khal, A., et al. (2021). SARS-CoV-2 seroprevalence in the urban population of Qatar: an analysis of antibody testing on a sample of 112,941 individuals. iScience *24*, 102646. https://doi.org/10.1016/j.isci.2021.102646.

Ehtezazi, T., Evans, D.G., Jenkinson, I.D., Evans, P.A., Vadgama, V.J., Vadgama, J., Jarad, F., Grey, N., and Chilcott, R.P. (2021). SARS-CoV-2: characterisation and mitigation of risks associated with aerosol generating procedures in dental practices. Br. Dent. J. *230*, 1–7. https://doi.org/10.1038/s41415-020-2504-8.

Gao, Q., Bao, L.L., Mao, H.Y., Wang, L., Xu, K.W., Yang, M.N., Li, Y.J., Zhu, L., Wang, N., Lv, Z., et al. (2020). Development of an inactivated vaccine candidate for SARS-CoV-2. Science *369*, 77–81. https://doi.org/10.1126/science.abc1932.

Gu, L., Meng, R., Tang, Y., Zhao, K., Liang, F., Zhang, R., Xue, Q., Chen, F., Xiao, X., Wang, H., et al. (2019). Toll-like receptor 4 signaling licenses

the cytosolic transport of lipopolysaccharide from bacterial outer membrane vesicles. Shock *51*, 256–265. https://doi.org/10.1097/shk.0000000000001129.

Hu, C.M.J., Fang, R.H., Wang, K.C., Luk, B.T., Thamphiwatana, S., Dehaini, D., Nguyen, P., Angsantikul, P., Wen, C.H., Kroll, A.V., et al. (2015). Nanoparticle biointerfacing by platelet membrane cloaking. Nature *526*, 118–121. https://doi.org/10.1038/nature15373.

Jan, A.T. (2017). Outer membrane vesicles (OMVs) of gram-negative bacteria: a perspective update. Front. Microbiol. *8*, 1053. https://doi.org/10.3389/fmicb.2017.01053.

Jeyanathan, M., Afkhami, S., Smaill, F., Miller, M.S., Lichty, B.D., and Xing, Z. (2020). Immunological considerations for COVID-19 vaccine strategies. Nat. Rev. Immunol. *20*, 615–632. https://doi.org/10.1038/s41577-020-00434-6.

Jiang, S., Bottazzi, M.E., Du, L., Lustigman, S., Tseng, C.-T.K., Curti, E., Jones, K., Zhan, B., and Hotez, P.J. (2012). Roadmap to developing a recombinant coronavirus S protein receptor-binding domain vaccine for severe acute respiratory syndrome. Expert Rev. Vaccines *11*, 1405–1413. https://doi.org/10.1586/erv.12.126.

Kaparakis-Liaskos, M., and Ferrero, R.L. (2015). Immune modulation by bacterial outer membrane vesicles. Nat. Rev. Immunol. *15*, 375–387. https://doi.org/10.1038/nri3837.

Krammer, F. (2020). SARS-CoV-2 vaccines in development. Nature *586*, 516–527. https://doi.org/10.1038/s41586-020-2798-3.

Kroll, A.V., Fang, R.H., Jiang, Y., Zhou, J., Wei, X., Yu, C.L., Gao, J., Luk, B.T., Dehaini, D., Gao, W., and Zhang, L. (2017). Nanoparticulate delivery of cancer cell membrane elicits multiantigenic antitumor immunity. Adv. Mater. *29*, 1703969. https://doi.org/10.1002/adma.201703969.

Laughlin, R.C., Mickum, M., Rowin, K., Adams, L.G., and Alaniz, R.C. (2015). Altered host immune responses to membrane vesicles from Salmonella and Gram-negative pathogens. Vaccine *33*, 5012–5019. https://doi.org/10.1016/j.vaccine.2015.05.014.

Le, Q.-V., Lee, J., Lee, H., Shim, G., and Oh, Y.-K. (2021). Cell membrane-derived vesicles for delivery of therapeutic agents. Acta Pharm. Sin. B *11*, 2096–2113. https://doi.org/10.1016/j.apsb.2021.01.020.

Lee, E.Y., Choi, D.S., Kim, K.P., and Gho, Y.S. (2008). Proteomics in gram-negative bacterial outer membrane vesicles. Mass Spectrom. Rev. *27*, 535–555. https://doi.org/10.1002/mas.20175.

Liu, C., Zhou, Q.Q., Li, Y.Z., Garner, L.V., Watkins, S.P., Carter, L.J., Smoot, J., Gregg, A.C., Daniels, A.D., Jervey, S., and Albaiu, D. (2020). Research and development on therapeutic agents and vaccines for COVID-19 and related human coronavirus diseases. ACS Cent. Sci. *6*, 315–331. https://doi.org/10.1021/acscentsci.0c00272.

Lycke, N. (2012). Recent progress in mucosal vaccine development: potential and limitations. Nat. Rev. Immunol. *12*, 592–605. https://doi.org/10.1038/nri3251.

MacLennan, I.C.M., and Vinuesa, C.G. (2002). Dendritic cells, BAFF, and APRIL: innate players in adaptive antibody responses. Immunity *17*, 235–238. https://doi.org/10.1016/s1074-7613(02)00398-9.

McKenzie, B.S., Corbett, A.J., Brady, J.L., Dyer, C.M., Strugnell, R.A., Kent, S.J., Kramer, D.R., Boyle, J.S., and Lew, A.M. (2001). Nucleic acid vaccines: tasks and tactics. Immunol. Res. *24*, 225–244. https://doi.org/10.1385/ir:24:3:225.

Mi, Z., Feng, Z.-C., Li, C., Yang, X., Ma, M.-T., and Rong, P.-F. (2019). Salmonella-mediated cancer therapy: an innovative therapeutic strategy. J. Cancer *10*, 4765–4776. https://doi.org/10.7150/jca.32650.

Mond, J.J., and Brunswick, M. (2003). Proliferative assays for B cell function. Curr. Protoc. Immunol. *Chapter 3*. https://doi.org/10.1002/0471142735.im0310s57.

Mulcahy, L.A., Pink, R.C., and Carter, D.R.F. (2014). Routes and mechanisms of extracellular vesicle uptake. J. Extracell. Vesicles *3*, 24641. https://doi.org/10.3402/jev.v3.24641.

Nothelfer, K., Sansonetti, P.J., and Phalipon, A. (2015). Pathogen manipulation of B cells: the best defence is a good offence. Nat. Rev. Microbiol. *13*, 173–184. https://doi.org/10.1038/nrmicro3415.

O'Donoghue, E.J., Sirisaengtaksin, N.A.-O.X., Browning, D.F., Browning, D.A.-O., Bielska, E.A.-O., Hadis, M., Fernandez-Trillo, F.A.-O., Alderwick, L., Jabbari, S.A.-O., Krachler, A.M., and Krachler, A.A.-O. (2017). Lipopolysaccharide structure impacts the entry kinetics of bacterial outer membrane vesicles into host cells. PLoS Pathog. *13*, e1006760. https://doi.org/10.1371/journal.ppat.1006760.

Ols, S., and Loré, K. (2019). Imaging the early fate of mRNA vaccines. Nat. Biomed. Eng. *3*, 331–332. https://doi.org/10.1038/s41551-019-0399-y.

Palucka, K., and Banchereau, J. (2012). Cancer immunotherapy via dendritic cells. Nat. Rev. Cancer *12*, 265–277. https://doi.org/10.1038/nrc3258.

Pushparajah, D., Jimenez, S., Wong, S., Alattas, H., Nafissi, N., and Slavcev, R.A. (2021). Advances in gene-based vaccine platforms to address the COVID-19 pandemic. Adv. Drug Deliv. Rev. *170*, 113–141. https://doi.org/10.1016/j.addr.2021.01.003.

Qin, F., Xia, F., Chen, H., Cui, B., Feng, Y., Zhang, P., Chen, J., and Luo, M. (2021). A guide to nucleic acid vaccines in the prevention and treatment of infectious diseases and cancers: from basic principles to current applications. Front. Cell Dev. Biol. *9*, 633776. https://doi.org/10.3389/fcell.2021.633776.

Ren, E., Liu, C., Lv, P., Wang, J., and Liu, G. (2021). Genetically engineered cellular membrane vesicles as tailorable shells for therapeutics. Adv. Sci. *8*, e2100460. https://doi.org/10.1002/advs.202100460.

Rothe, C., Schunk, M., Sothmann, P., Bretzel, G., Froeschl, G., Wallrauch, C., Zimmer, T., Thiel, V., Janke, C., Guggemos, W., et al. (2020). Transmission of 2019-nCoV infection from an asymptomatic contact in Germany. N. Engl. J. Med. *382*, 970–971. https://doi.org/10.1056/nejmc2001468.

Sachsenberg, N., Perelson, A.S., Yerly, S., Schockmel, G.A., Leduc, D., Hirschel, B., and Perrin, L. (1998). Turnover of CD4+ and CD8+ T lymphocytes in HIV-1 infection as measured by Ki-67 antigen. J. Exp. Med. *187*, 1295–1303. https://doi.org/10.1084/jem.187.8.1295.

Schetters, S.T.T., Jong, W.S.P., Horrevorts, S.K., Kruijssen, L.J.W., Engels, S., Stolk, D., Daleke-Schermerhorn, M.H., Garcia-Vallejo, J., Houben, D., Unger, W.W.J., et al. (2019). Outer membrane vesicles engineered to express membrane-bound antigen program dendritic cells for cross-presentation to CD8(+) T cells. Acta Biomater. *91*, 248–257. https://doi.org/10.1016/j.actbio.2019.04.033.

Schwechheimer, C., and Kuehn, M.J. (2015). Outer-membrane vesicles from Gram-negative bacteria: biogenesis and functions. Nat. Rev. Microbiol. *13*, 605–619. https://doi.org/10.1038/nrmicro3525.

Shibuya, M., Tamiya, S., Kawai, A., Hirai, T., Cragg, M.S., and Yoshioka, Y. (2021). Synergistic effect of non-neutralizing antibodies and interferon-γ for cross-protection against influenza. iScience *24*, 103131. https://doi.org/10.1016/j.isci.2021.103131.

Shin, M.D., Shukla, S., Chung, Y.H., Beiss, V., Chan, S.K., Ortega-Rivera, O.A., Wirth, D.M., Chen, A., Sack, M., Pokorski, J.K., and Steinmetz, N.F. (2020). COVID-19 vaccine development and a potential nanomaterial path forward. Nat. Nanotechnol. *15*, 646–655. https://doi.org/10.1038/s41565-020-0737-y.

Thomas, P., and Smart, T.G. (2005). HEK293 cell line: a vehicle for the expression of recombinant proteins. J. Pharmacol. Toxical. Methods *51*, 187–200. https://doi.org/10.1016/j.vascn.2004.08.014.

van der Donk, L.E.H., Eder, J., van Hamme, J.L., Brouwer, P.J.M., Brinkkemper, M., van Nuenen, A.C., van Gils, M.J., Sanders, R.W., Kootstra, N.A., Bermejo-Jambrina, M., et al. (2021). SARS-CoV-2 infection activates dendritic cells via cytosolic receptors rather than extracellular TLRs. Preprint at bioRxiv. https://doi.org/10.1101/2021.09.02.458667.

Villadangos, J.A., and Schnorrer, P. (2007). Intrinsic and cooperative antigen-presenting functions of dendritic-cell subsets in vivo. Nat. Rev. Immunol. *7*, 543–555. https://doi.org/10.1038/nri2103.

Walker, P.G.T., Whittaker, C., Watson, O.J., Baguelin, M., Winskill, P., Hamlet, A., Djafaara, B.A., Cucunubá, Z., Olivera Mesa, D., Green, W., et al. (2020). The impact of COVID-19 and strategies for mitigation and suppression in low- and middle-income countries. Science *369*, 413–422. https://doi.org/10.1126/science.abc0035.

Wang, N., Shang, J., Jiang, S.B., and Du, L.Y. (2020). Subunit vaccines against emerging pathogenic human coronaviruses. Front. Microbiol. *11*, 298. https://doi.org/10.3389/fmicb.2020.00298.

Wu, F., Zhao, S., Yu, B., Chen, Y.M., Wang, W., Song, Z.G., Hu, Y., Tao, Z.W., Tian, J.H., Pei, Y.Y., et al. (2020). A new coronavirus associated with human respiratory disease in China. Nature *579*, 265–269. https://doi.org/10.1038/s41586-020-2008-3.

Xie, F., Su, P., Pan, T., Zhou, X., Li, H., Huang, H., Wang, A., Wang, F., Huang, J., Yan, H., et al. (2021). Engineering extracellular vesicles enriched with palmitoylated ACE2 as COVID-19 therapy. Adv. Mater. *33*, 2103471. https://doi.org/10.1002/adma.202103471.

Zhang, P., Chen, Y., Zeng, Y., Shen, C., Li, R., Guo, Z., Li, S., Zheng, Q., Chu, C., Wang, Z., et al. (2015). Virus-mimetic nanovesicles as a versatile antigen-delivery system. Proc. Natl. Acad. Sci. U S A *112*, E6129–E6138. https://doi.org/10.1073/pnas.1505799112.

Zhou, P., Yang, X.-L., Wang, X.-G., Hu, B., Zhang, L., Zhang, W., Si, H.-R., Zhu, Y., Li, B., Huang, C.-L., et al. (2020a). A pneumonia outbreak associated with a new coronavirus of probable bat origin. Nature *579*, 270–273. https://doi.org/10.1038/s41586-020-2012-7.

Zhou, X., Jiang, X., Qu, M., Aninwene, G.E., Jucaud, V., Moon, J.J., Gu, Z., Sun, W., and Khademhosseini, A. (2020b). Engineering antiviral vaccines. ACS Nano *14*, 12370–12389. https://doi.org/10.1021/acsnano.0c06109.

Zhu, N., Zhang, D.Y., Wang, W.L., Li, X.W., Yang, B., Song, J.D., Zhao, X., Huang, B.Y., Shi, W.F., Lu, R.J., et al. (2020). A novel coronavirus from patients with pneumonia in China, 2019. N. Engl. J. Med. *382*, 727–733. https://doi.org/10.1056/nejmoa2001017.

Zou, M.-Z., Li, Z.-H., Bai, X.-F., Liu, C.-J., and Zhang, X.-Z. (2021). Hybrid vesicles based on autologous tumor cell membrane and bacterial outer membrane to enhance innate immune response and personalized tumor immunotherapy. Nano Lett. *21*, 8609–8618. https://doi.org/10.1021/acs.nanolett.1c02482.

STAR★METHODS

KEY RESOURCES TABLE

REAGENT or RESOURCE	SOURCE	IDENTIFIER
Antibodies		
SARS-CoV-2 Spike S1 rabbit monoclonal antibody	Sino Biological Inc.	Cat# 40150-R007; RRID:AB_2827979
FITC-conjugated goat anti-rabbit IgG (H + L)	Abcam	Cat# ab6717; RRID:AB_955238
HRP-conjugated goat anti-mouse IgG (H + L)	Abcam	Cat# ab6789; RRID:AB_955439
HRP-conjugated goat anti-mouse IgG1	Abcam	Cat# ab97240; RRID:AB_10695944
HRP-conjugated goat anti-mouse IgG2a	Abcam	Cat# ab97245; RRID:AB_10680049
anti-mouse CD16/CD32 (clone 93)	Biolegend	Cat# 101302; RRID:AB_312801
PE/Cy7 anti-mouse B220 (clone RA3-6B2)	Biolegend	Cat# 103222; RRID:AB_313005
FITC anti-mouse CD69 (clone H1.2F3)	Biolegend	Cat# 104505; RRID:AB_313108
FITC anti-mouse Ki67 (clone SolA15)	Biolegend	Cat# 652410; RRID:AB_2562141
FITC anti-mouse CD4 (clone GK1.5)	Biolegend	Cat# 100406; RRID:AB_312691
Percp/Cy5.5 anti-mouse CD11b (clone M1/70)	Biolegend	Cat# 101228; RRID:AB_893232
APC anti-mouse CD86 (clone 24F)	Biolegend	Cat# 105012; RRID:AB_493342
APC anti-mouse CD138 (clone 281-2)	Biolegend	Cat# 142506; RRID:AB_10962911
PE/Cy7 anti-mouse I-A/I-E (MHC II) (clone M5/114.15.2)	Biolegend	Cat# 107630; RRID:AB_2069376
FITC anti-mouse CD11c (clone N418)	Biolegend	Cat# 117306; RRID:AB_313775
Percp/Cy5.5 anti-mouse CD3 (clone 145-2C11)	Biolegend	Cat# 100328; RRID:AB_893318
APC anti-mouse CD4 (clone GK1.5)	Biolegend	Cat# 100411; RRID:AB_312696
PE anti-mouse CD80 (clone 16-10A1)	eBioscience	Cat# 12-0801-85; RRID:AB_465754
PE/Cy7 anti-mouse IFNγ (clone XMG1.2)	Biolegend	Cat# 505825; RRID:AB_1595591
PE anti-mouse anti-His tag (clone J095G46)	Biolegend	Cat# 362603; RRID:AB_2563634
PE/Cy7 anti-mouse H-2Kb/H-2Db (MHC-I) (clone 28-8-6)	Biolegend	Cat# 114616; RRID:AB_2750196
PE anti-mouse CD8 (clone 53-6.7)	Biolegend	Cat# 100708; RRID:AB_312747
rabbit anti-Na+/K+ ATPase monoclonal antibody	ABclonal	Cat# A11683; RRID:AB_2861628
rabbit anti-SARS-CoV-2 Spike S1 polyclonal antibody	ABclonal	Cat# A20136; RRID:AB_2862928
Bacterial and virus strains		
Attenuated salmonella typhimurium VNP20009	ATCC	202165
Chemicals, peptides, and recombinant proteins		
Recombinant murine GM-CSF	PeproTech	315-03
Recombinant SARS-CoV-2 S1 protein	Sino Biological Inc.	40591-V08H
Polyetherimide (PEI, average MW 25000)	Sigma-Aldrich	408727
3,3′-dioctadecyloxacarbocyanine perchlorate (DiO)	Beyotime	C1038
Hoechst 33342	Beyotime	C1028
Protease inhibitor cocktail (100×)	Thermo Scientific	78429
Cyanine5.5 NHS ester	Lumiprobe	17020
Critical commercial assays		
BCA protein assay kit	Beyotime	P0010
Coomassie Blue Fast Staining Solution	Beyotime	P0017
ECL luminescence reagent	Sangon Biotech	C510043
CCK-8 kit	Beyotime	C0038
TMB chromogen solution	Sangon Biotech	E661007-0100

(*Continued on next page*)

Continued

REAGENT or RESOURCE	SOURCE	IDENTIFIER
Foxp3/transcription factor fixation/ permeabilization concentrate and diluent	eBioscience	00-5521-00
Mouse IL-6 ELISA Kit	Multi Sciences	70-EK206/3-96
Mouse IFN-γ ELISA Kit	Multi Sciences	70-EK280/3-96
Experimental models: Cell lines		
Mouse: DC2.4	Sigma	SCC142
Human: HEK 293T	ATCC	CRL-3216
Experimental models: Organisms/strains		
Mouse: C57BL/6J	Shanghai Jiesijie Laboratory Animal Co., Ltd	N/A
Software and algorithms		
GraphPad Prism 7	GraphPad Software Inc.	https://www.graphpad.com/
FlowJo X 10.0	FlowJo	https://www.flowjo.com/
ImageJ 1.52a	ImageJ	https://imagej.nih.gov/ij/
Leica Application Suite X	Leica	https://www.leica-microsystems.com.cn/
K-Viewer 1.5.3.1	KFBIO	http://www.kfbio.cn/

RESOURCE AVAILABILITY

Lead contact

Further information and requests for resources and reagents should be directed to and will be fulfilled by the lead contact, Jinyao Liu (jyliu@sjtu.edu.cn).

Materials availability

This study did not generate new unique materials.

Data and code availability

This study did not generate and analyze any datasets or code. All data are included in the article and supplemental information and any additional information will be available from the lead contact upon request.

EXPERIMENTAL MODEL AND SUBJECT DETAILS

Cell culture and transfection with spike protein

Human embryonic kidney (HEK) 293T cells were obtained from American Type Culture Collections (ATCC) and cultured in Dulbecco's modified Eagle's medium (DMEM) supplemented with 10% fetal bovine serum (FBS) and 1% antibiotics (penicillin-streptomycin) in a humidified atmosphere incubator with 5% CO_2 at 37°C.

HEK 293T cells were transiently transfected with plasmid encoding spike protein using polyetherimide (PEI, average MW 25000). The sequence of the spike protein was shown in Table S1. The truncated sequence was insert downstream of cytomegalovirus promoter into PCDNA3.1 plasmid. When cells grew to 70% in a 10 cm culture dish, PEI-DNA complex containing 10 μg plasmid and 30 μg PEI in 500 μL PBS was added to the culture medium. The cells were harvested at 48 h post transfection for following experiments.

Bacterial culture and OMVs collection

Attenuated *Salmonella typhimurium* VNP20009 strain was cultured on Luria Bertani (LB) agar plate at 37°C. Then a single colony was inoculated into LB liquid medium with 100 μg/mL kanamycin. Overnight culture was diluted 1:100 to fresh LB medium with 100 μg/mL kanamycin and incubated at 37°C for 20 h with shaking at 200 rpm. Bacterial medium was centrifuged at 9000 rpm for 30 min to remove VNP20009 and then supernatant was filtered through 0.45 μm filters (Millipore, USA). The filtrate was ultracentrifuged at 170000 g for 1 h at 4°C, and purified by washing with PBS twice. OMVs were resuspended in PBS and stored at −80°C for further experiments.

Cell viability assay

Cell viability was detected by a CCK-8 (Beyotime, China) and DC2.4 cells were used as a model cell line. DC2.4 cells were cultured in RPMI 1640 medium supplemented with 10% FBS and 1% antibiotics (penicillin-streptomycin) at 37°C in 5% CO_2. DC2.4 cells (8×10^3 cells/well) were inoculated into a 96-well plate and allowed to adhere overnight. Then cells were treated with serially diluted HMVs in 37°C for 24 h. 10 μL of CCK-8 solution was added into each well. After 4 h incubation, the absorbance was measured at 450 nm using a microplate reader (Bio Tek, USA). Cell viability was calculated as the ratio of each experimental group to the control.

Cell uptake *in vitro*

DC2.4 cells were seeded at a density of 2×10^5 cells in glass bottom cell culture dishes. Membrane vesicles were labeled with Cy5.5-NHS ester. DC2.4 cells were treated with equal amount of SMVs, OMVs and HMVs, respectively. After 10 h incubation, cells were collected and labeled with Hoechst 33342 (Beyotime, China). Subsequently, the cells were washed with PBS for three times and imaged by LSCM. For quantitative analysis of cell uptake, the cells were collected after incubation for 0, 2, 4, 6, 8, and 10 h by flow cytometric analysis.

Maturation and activation of BMDCs *in vitro*

The legs of C57BL/6 male mice (6-8 weeks old) were separated. The bone marrow was flushed out with RPMI-1640 by 1 mL syringe and centrifuged at 1500 rpm for 3 min. Then cells were cultured in RPMI-1640 containing 10% FBS, 1% penicillin-streptomycin and 20 ng/mL granulocyte macrophage colony-stimulating factor (GM-CSF) (PeproTech, UK) with 5% CO_2 at 37°C. Half of the medium was removed on day 3 and an additional culture medium with GM-CSF (20 ng/mL) was added. BMDCs were harvested on day 6-8 and transferred to a 12-well plate at a density of 2×10^5 cells per well. Cells were treated with SMVs (20 μg), OMVs (2 μg), and HMVs (20 μg) with equivalent protein for 24 h, respectively. PBS-treated cells were used as blank control. Cells were then collected, washed, and blocked with anti-mouse CD16/32 (BioLegend). For specific labeling, cells were stained with anti-mouse antibody against CD11c-FITC (N418, BioLegend), CD11b-Percp/Cy5.5 (M1/70, BioLegend), CD80-PE (16-10A1, eBioscience), CD86-APC (24F, BioLegend), $H\text{-}2K^b$/$H\text{-}2D^b$ (MHC-I)-PE/Cy7 (28-8-6, BioLegend) and I-A/I-E (MHC-II) -PE/Cy7 (M5/114.15.2, BioLegend) in 0.5% bovine serum albumin (BSA) dissolved in PBS on ice for 40 min. After washing with PBS for 3 times, cells were analyzed by flow cytometry.

Mice vaccination

Specific pathogen-free (SPF) female C57BL/6 mice at 6-8 weeks of age were purchased from Jiesijie (Shanghai, China) and divided into four groups randomly (n = 6 per group). On days 0, 7, 14, mice were immunized subcutaneously with SMVs (1 mg), OMVs (10 μg), and HMVs (1 mg, SMVs/OMVs = 100:1) in 200 μL PBS, respectively. The control group was injected with PBS. Serum was collected on days 14, 21, and 28 for IgG antibodies assessment. The body weight of mice was recorded every three days since the first immunization. Mice were euthanatized on day 30. Lymph nodes, spleen, and serum were collected for evaluation of immune responses by flow cytometry. All animal experiments were conducted by the Institutional Animal Care and Use Committee guidelines of Shanghai Jiao Tong University.

METHOD DETAILS

Flow cytometric analysis of spike protein expression

HEK 293T cells were collected at 48 h post transfection. HEK 293T cells without transfection were used as a control. After washing with PBS, cells were incubated with SARS-CoV-2 Spike S1 rabbit monoclonal antibody (1:200) (Sinobiological, China) for 1 h on ice, followed by FITC-conjugated goat anti-rabbit IgG (1:1000) (Abcam, UK) for 1 h. After washing with PBS, cells were analyzed by flow cytometry.

Preparation of SMVs and HMVs

For cell membrane vesicles, HEK 293T cells transfected with Spike protein were collected and washed twice with PBS. Then cells were resuspended in a hypotonic solution (1 mM $NaHCO_3$, 0.2 mM EDTA, 75 mM sucrose and protease inhibitor in ultrapure water) on ice for 30 min. The solution was broken under ultrasonication at 200 W for 3 min (3 s on, 3 s off) and centrifuged at 4000 rpm at 4°C for 5 min to remove cells. The supernatant was then centrifuged at 15000 rpm at 4°C for 30 min and washed with PBS to collect SMVs, which were stored in PBS at −80°C for further experiments. The protein concentration was quantified using

a BCA protein assay kit (Beyotime, China). SMVs and OMVs were mixed at a mass ratio of 10:1 in PBS and crushed by ultrasound to facilitate membrane fusion. Finally, the mixture was extruded 14 times through a 200 nm polycarbonate porous membrane by using a mini extruder (Avavti Polar Lipids, USA).

Characterization of SMVs, OMVs, and HMVs

Hydrodynamic size and surface zeta potential of vesicles were measured by dynamic light scattering (DLS) on a Zetasizer Nano ZS (Malvern, UK). For nano-tracking analyses, vesicles were diluted in PBS and 60 s videos were recorded using camera level 14. The data was analyzed using NTA software with the detection threshold 4. The structure of vesicles was observed using a transmission electron microscope (TEM, Hitachi, Japan). 10 μL solution was deposited onto a carbon-coated 400-mesh copper grid. After standing for 15 min, the sample was washed with ddH_2O twice and negatively stained with 1% phosphotungstic acid hydrate for 1 min. SMVs were labeled with DiO and OMVs were labeled with Cy5.5. HMVs were visualized under LSCM with a 63 × oil objective (Leica TCS SP8, German). At the same time, the vesicles were detected by flow cytometry using FITC and APC-A700 channels. Membrane proteins were characterized by sodium dodecyl sulfate-polyacrylamide gel electrophoresis (SDS-PAGE) and western blot analysis. Total protein contents of SMVs, OMVs, and HMVs were quantified by a BCA protein assay kit. Membrane vesicles (20 μg/sample) mixed with SDS-PAGE loading buffer were boiled at 95°C for 10 min and separated in a 4-15% Precast-Glgel. The quantification of molecular weight was performed using a prestained protein ladder (Thermo Scientific, USA, 10 to 250 kDa). Protein was stained with Coomassie Blue Fast Staining Solution (Beyotime, China) and imaged after destaining. Then protein was transferred onto polyvinylidene fluoride (PVDF) membranes by Trans-Blot Turbo (Bio-Rad, USA). After blocking with 5% nonfat-dried milk at 25°C for 1 h, the membranes were incubated with primary antibodies: rabbit anti-SARS-CoV-2 Spike S1 polyclonal antibody (1:1000) (ABclonal, China) and rabbit anti-Na^+/K^+ ATPase monoclonal antibody (1:1000) (ABclonal, China) at 4°C overnight. The membranes were further incubated with secondary antibody: HRP Goat Anti-Rabbit IgG (H + L) (1:10000) (ABclonal, China) at room temperature for 1 h. After rinsing with TBST for three times, membranes were visualized with ECL luminescence reagent (Sangon Biotech, China) by Amersham Imager 680 (GE Analytical Instruments, USA).

ELISA for serum antibody titer evaluation

SARS-CoV-2 S1 specific IgG titers were determined by ELISA. 2 μg/mL recombinant SARS-CoV-2 S1 protein (Sino Biological, China) in carbonate buffer solution (pH 9.6) was incubated in 96-well ELISA plates (100 μL/well) overnight at 4°C. After rinsing with washing buffer (0.05% Tween-20 in PBS) for three times, the plates were blocked with 1% BSA dissolved in PBS at room temperature for 2 h. Serial 2-fold dilutions of sera (100 μL/well) in dilution buffer (0.5% BSA in PBS) was added and the plates were incubated for 1 h at 37°C. Then horseradish peroxidase (HRP)-conjugated goat anti-mouse IgG, IgG1 or IgG2a (Abcam, 1:100000) was added to plates (100 μL/well) and incubated for 1 h at room temperature. After rinsing with washing buffer for three times, the plates were incubated with TMB chromogen solution (Sangon Biotech, 200 μL/well) at 37°C for 20 min. Then the reaction was stopped with stopping solution (0.5 M H_2SO_4, 50 μL/well). Finally, the absorbance at 450 nm was read using a microplate reader (Bio Tek, USA). The endpoint titers were defined as the highest serum dilution which ≥ 2-fold over the absorbance of the background.

Immune responses and flow cytometric analysis *in vivo*

Lymph nodes and spleen tissues were collected after mice were euthanatized on day 30. Single cells were obtained by grinding tissues with 70 μm nylon filters in 0.5% BSA-PBS. Anti-mouse antibodies against CD3-Percp/Cy5.5 (145-2C11, BioLegend), CD4-APC (GK1.5, BioLegend), CD4-FITC (GK1.5, BioLegend), CD8-PE (53-6.7, BioLegend), CD11c-FITC (N418, BioLegend), CD11b-Percp/Cy5.5 (M1/70, BioLegend), CD80-PE (16-10A1, eBioscience), CD86-APC (24F, BioLegend), CD69-FITC (H1.2F3, BioLegend), B220-Percp/Cy5.5 (RA3-6B2, BioLegend), CD138-APC (281-2, BioLegend) or I-A/I-E (MHC II)-PE/Cy7 (M5/114.15.2, BioLegend) were used for cell surface antigen staining. After washing with PBS for three times, cells were treated with Foxp3/transcription factor fixation/permeabilization concentrate and diluent (eBioscience, USA) and incubated with anti-mouse antibodies against IFNγ-PE/Cy7 (XMG1.2, BioLegend) or Ki67-FITC (SolA15, BioLegend) for intracellular antigen staining. Besides, S1 protein with His tag (Sino Biological, China) and anti-His tag-PE (BioLegend) were used to label S1 specific B cells. The cells were analyzed by flow cytometry.

ELISA for detection of cytokines in serum

Mice were euthanized at day 30 and serum samples were collected for quantification of IL-6 and IFN-γ by ELISA kit according to instructions and calculated by the standard curves on the basis of standard samples.

Histopathology assay

For histopathology, tissues of the liver, spleen, lung, and kidney from mice were fixed in 4% paraformaldehyde (PFA), embedded in paraffin, sectioned, and stained with hematoxylin and eosin (H&E). The tissue slides were visualized under scanning microscope and analyzed with K-viewer software. Original magnification was 10×.

QUANTIFICATION AND STATISTICAL ANALYSIS

All data was analyzed with GraphPad Prism 7.0 software. Unless specified, data are presented as mean ± SD in all experiments. An unpaired Student's t test, one-way analysis of variance (ANOVA) with the Tukey's comparison post-test or two-way ANOVA with the Bonferroni correction post-test were used to determine statistical significance among different groups (*$p < 0.05$; **$p < 0.01$; ***$p < 0.001$; ****$p < 0.0001$).